Microanalysis of Dust Deposition inside Emperor Qin's Terra-Cotta Warriors and Horses Museum

Tafeng Hu[1,2,3], Junji Cao[1,2]*, Shuncheng Lee[3], Xuxiang Li[1], Zhenxing Shen[1], Bo Rong[4], Zhisheng An[2]

[1] *Department of Environmental Science and Engineering, Xi'an Jiaotong University, Xi'an, China*
[2] *SKLLQG, Institute of Earth Environment, Chinese Academy of Sciences, Xi'an, China*
[3] *Department of Civil and Structural Engineering, The Hong Kong Polytechnic University, Hong Kong, China*
[4] *Emperor Qin's Terra-cotta Warriors and Horses Museum, Xi'an, China*

ABSTRACT

Indoor dust deposition, including long-term (>10 years) deposition, short-term (~0.5 year) deposition, and pigment flake samples from partially restored warriors were collected in Emperor Qin's Terra-cotta Warriors and Horses Museum in Xi'an, Shaanxi Province, China. Morphological and elemental analyses of individual particles were performed with scanning electron microscopy and energy dispersive X-ray spectrometry to investigate their composition and potential to damage the statues. Most of the indoor dust was composed of clay minerals, fly ash, and biogenic particles. Particles in 51.5% of the short-term deposition, and 49.5% of the long-term deposition contained elemental sulfur. Particles which contained sulfur were mostly associated with calcium sulfate in an internally mixed state with clay or quartz. Crystals of calcium sulfate were also found near interconnected pits and cracks on the outer surface of pigment flakes, revealing an acidic chemical reaction between sulfur dioxide and pigment material or deposited particles as the cause of pits and cracks on the statues' faces.

Keywords: Dust deposition; Terra-cotta warriors; Museum; Scanning electron microscopy.

INTRODUCTION

The conservation of cultural heritage and its protection against possible damage from air pollution is of increasing scientific concern (Brimblecombe, 1990; Nazaroff and Cass, 1991; Yoon and Brimblecombe, 2001; Brimblecombe, 2003). Air pollution can cause chemical damage or soiling of surfaces due to particle deposition or absorption of gases (De Bock *et al.*, 1995; Van Grieken *et al.*, 1998). Damage also occurs when soiled objects are subjected to aggressive and frequent cleaning. Dust is abrasive and can carry harmful substances to the surfaces of artwork (Katsanos *et al.*, 1999; Nazaroff and Cass, 1991; Yoon and Brimblecombe, 2001). Investigations on calcareous stone weathering show that physical stress from soluble salt crystallization in pores caused stone breakage (Cardell *et al.*, 2003).

The discovery of terra-cotta warriors in 1974 was one of the most important archeological findings of the 20th

century. Today, the terra-cotta warriors and horses inside the largest on-site museum in China are recognized as the "Eighth Wonder of the World". More than 2 million tourists visit the museum each year. Since their excavation, these priceless and irreplaceable statues have undergone changes in their appearance after more than 30 years of exposure in the exhibition halls (Zhang, 1998; Cao *et al.*, 2005a). The Emperor Qin's Terra-cotta Warriors and Horses Museum (QTM) is located 30 km to the east of Xi'an, a city of eight million people with increasing traffic, high coal consumption, and intensive building construction. The museum is also surrounded by agricultural fields in which biomass is periodically burned.

Once particles deposit on works of art, their appearance and chemical interactions with the surface depend on their chemical composition and morphology (Nazaroff *et al.*, 1993). To investigate soiling and corrosive hazards posed by dry-deposited particles on the artifacts of the QTM, long-term (>10 years) deposition, short-term (~0.5 year) deposition, and pigment flakes were collected in Pit No.1 Exhibition Hall (Pit 1). Size, morphology, and chemical composition of individual particles in these samples were determined by scanning electron microscopy and energy dispersive X-ray spectrometry (SEM-EDX) to characterize dusts deposited inside the QTM and to estimate the

---
* Corresponding author. Tel.: 86-29-8832-6488;
 Fax: 86-29-8832-0456
 E-mail address: cao@loess.llqg.ac.cn

potential hazards of dust particles in relation to the statues.

METHODOLOGY

Sample Collection

There is a restoration area at the rear of Pit 1, the largest exhibition hall of QTM. Thousands of terra-cotta shards excavated in the 1970s and 1980s were placed in lines on plastic sheets, some of which are too small to be relocated and restored. Undisturbed gray dust that has accumulated on the shards and plastic sheets for more than 10 years was collected as long-term (>10 years) deposition. Six samples were swept into plastic scoops with soft-bristle brushes and put into self-sealed plastic bags during April 2006. Four flakes, representative of remnants of the white pigment applied 2000 years ago, were removed with forceps from the faces of partially restored statues.

The Restoration Department of QTM cleans the statues with brushes twice a year. Two shoulders of warrior statues in the middle of Pit 1, with no pigment remnants, were selected to collect deposits for six months after being cleaned in September 2005. Two clean porcelain enamel plates were placed on the ground near the sampled warriors to collect dust not affected by the statues. Dust deposited on the shoulders and in the plates was obtained as short-term (~0.5 year) deposition in March 2006. The shoulders showed a uniform and smooth surface after sweeping. After sampling, long-term deposition, short-term deposition, and pigment flake samples were sealed and stored in a refrigerator at 4°C until they were analyzed.

Sample Analyses

Samples were dispersed onto conductive double-sided adhesive carbon tape fixed on an aluminum sample holder. Overlapping particles were removed using a rubber pipette bulb. Pigment flakes were fixed to aluminum sample stubs with conductive adhesive carbon tape. Samples were coated under vacuum with platinum and analyzed with a JEOL JSM-6460 LV SEM (Japan Electron Optics Laboratory Co. Ltd., JP). For each sample, 10 secondary electron images (SEI) were acquired with magnifications from 3000× to 10000×, depending on the particle size. Sizes of individual particles were measured from their SEM images with JEOL SMILEVIEW 2.05 software. The diameter of a particle was estimated as the average of the longest dimension and its orthogonal width (Zhang *et al.*, 2003; Okada and Kai, 2004). All particles larger than 0.2 μm in each image were measured to obtain general size distributions. All individual particles larger than 0.5 μm were selected for elemental analyses using a NORAN SYSTEM SIX Si-Li EDX detector with an ultra-thin window (Thermo Electron Corporation, USA). The EDX counting time was 100 s live-time for each particle. X-ray peak intensities for each element were converted into weight fractions using the atomic number, absorption, and fluorescence correction of the EDX software.

RESULTS AND DISCUSSION

Types of Indoor Particles

Low atomic number particles with dominant C and O peaks in their spectra were designated as soot or biogenic particles, according to their particulate morphologies as soot consisting of chain or aggregate spheres and biogenic particles containing regular surface or symmetrical shapes. Identification of mineral dust particles with dominant inorganic elements is based on their elemental compositions by excluding C and O peaks from the spectra to avoid interference from the conductive carbon tape. Particles were classified into six X-rich groups, where element X has the maximum weight fraction, P(X), among the 10 most frequently detected inorganic elements (Okada and Kai, 2004), and $P(X) = X / (Na + Mg + Al + Si + S + K + Ca + Ti + Mn + Fe)$. Particles in each X-rich group were divided into X-dominant or $X_1 + X_2 + … + X_N$ subgroups, where $P(X) \geq 0.65$, or $P(X_1) + P(X_2) + … + P(X_N) \geq 0.65$. Using the 65% threshold, the particles were classified and their number percentages are shown in Table 1. The sum of the abundances in Table 1 is not 100% because fewer than 4% of particles in all the samples were unidentified with detectable elements that do not fall into any defined types.

Mineral particles were present in high number fractions (> 90%) in all dust samples. Si-rich particles accounted for 62.1–63.1% of the total particle numbers. Most of the Si-rich particles also contained elemental Al, indicating that Si-rich particles were mainly composed of quartz, silicates and aluminosilicates. Ca-rich particles contributed 25.6–26.9% of the total number with a Ca-dominant subgroup indicative of calcite, calces, and calcium hydroxide; the Ca + Mg subgroup indicative of dolomite; and Ca + S subgroup indicative of gypsum, bassanite, and anhydrite. The number fraction of Ca-dominant particles in short-term deposition (5.4%) is slightly higher than that in long-term deposition (4.3%). Ca + Si and Ca + Mg particle number fractions are also larger in short-term than in long-term deposition samples. Ca + S + Si particles were similar in both deposition samples. Other types such as Fe-rich, K-rich, and Ti-rich particles were summed less than 7% in all the samples.

As for particle size distribution and chemical composition, there is no difference between short-term deposition samples collected on the warriors' shoulders and in the porcelain enamel plates, nor between long-term deposition samples collected on shards and on the plastic sheets. The SEM resolution of ~0.2 μm imposed a physical limit to the detection of smaller particles. The vacuum associates with the sample preparation process may decrease the content of some volatile organic matter. The exclusion of C and O also underestimates the organic content of particles.

Particle Sources

The ratios of Ca mass fractions in individual mineral particles to Al and Si mass fractions are plotted in Fig. 1. The points in the diagrams represent individual mineral particles, among which Ca-containing components (calcite, dolomite, feldspar, and gypsum) are mixed internally with

Table 1. Individual particle types determined with short-term deposition and long-term deposition composition.

Type[c]	Short-term deposition (n = 390)[a]			Long-term deposition (n = 398)[a]		
	Averaged (wt%)[b]	Num.	Percentage (%)	Averaged (wt%)[b]	Num.	Percentage (%)
Si-rich		**242**	**62.1**		**251**	**63.1**
Si-dominant	Si (85 ± 11)	78	20.0	Si (84 ± 12)	103	25.9
Si + Al	Si (52 ± 6), Al (25 ± 5)	53	13.6	Si (53 ± 7), Al (24 ± 4)	45	11.3
Si + Al + Ca	Si(38 ± 5), Al (19 ± 4), Ca (18 ± 5)	18	4.6	Si (38 ± 5), Al (16 ± 4),Ca (17 ± 6)	12	3.0
Si + Al + Fe	Si(35 ± 6), Al (18 ± 3), Fe (19 ± 4)	18	4.6	Si (36 ± 5), Al (18 ± 3), Fe (20 ± 6)	10	2.5
Si + K	Si(54 ± 7), K (26 ± 5)	18	4.6	Si (56 ± 5), K (27 ± 6)	17	4.3
Si + Ca	Si(53 ± 7), Ca (23 ± 6)	19	4.9	Si (52 ± 8), Ca (24 ± 6)	14	3.5
Si + S + Ca	Si(35 ± 6), S (19 ± 3), Ca (23 ± 4)	18	4.6	Si (36 ± 6), S (20 ± 2), Ca (25 ± 5)	16	4.0
Si + others		20	5.1		34	8.7
Ca-rich		**105**	**26.9**		**102**	**25.6**
Ca-dominant	Ca (86 ± 12)	21	5.4	Ca (82 ± 8)	17	4.3
Ca + Mg	Ca (62), Mg (22)	1	1.3	Ca (58), Mg (42)	1	0.3
Ca + Si	Ca (46 ± 10), Si (28 ± 8)	16	4.1	Ca (53 ± 10), Si (20 ± 6)	4	1.0
Ca + S	Ca (51 ± 8), S (33 ± 5)	49	12.6	Ca (50 ± 7), S (34 ± 4)	62	15.6
Ca + S + Si	Ca (33 ± 3), S (21 ± 5), Si (25 ± 4)	18	4.6	Ca (34 ± 6), S (21 ± 4), Si (22 ± 4)	18	4.5
Fe-rich		**15**	**3.8**		**11**	**2.8**
Fe-dominant	Fe (89 ± 12)	5	1.3	Fe (81 ± 14)	4	1.0
Fe + Si	Fe (43 ± 10), Si (2 6± 4)	10	2.6	Fe (43 ± 10), Si (26 ± 4)	7	1.8
K-rich		**1**	**0.3**		**2**	**0.5**
K-dominant		0	0		0	0
K + S	K (61), S (39)	1	0.3	K (58 ± 7), S (39 ± 3)	2	0.5
Ti-rich		**2**	**0.5**		**2**	**0.5**
Ti-dominant	Ti (82)	1	0.3	Ti (72)	1	0.3
Ti + others	Ti (36), Si (27), Al (11)	1	0.3	Ti (35), Si (26), S (27)	1	0.3
S-rich		**4**	**1.0**		**7**	**1.8**
S-dominant		0	0	S (100)	1	0.3
S + Si + Ca	S (32 ± 3), Si (25 ± 4), Ca (30 ± 4)	3	0.8		0	0
S + Ca		0	0	S (50 ± 2), Ca (36 ± 8)	4	1.0
S + others		1	0.3		2	0.6
Low-Z	**C + O**	**12**	**3.1**	**C + O**	**7**	**1.8**
Total		**381**	**97.7**		**382**	**96.0**

Note: [a] n in parentheses are the total number of particles characterized in four short-term and six long-term deposition samples, respectively.

[b] Averaged weight percentage of measured elements and standard deviation.

[c] X-rich: particles with element X has the maximum weight fraction in spectra; X-dominant or $X_1 + X_2 + \ldots + X_N$: particles with the weight fractions of element X or $X_1 + X_2 + \ldots + X_N$ larger than 65%.
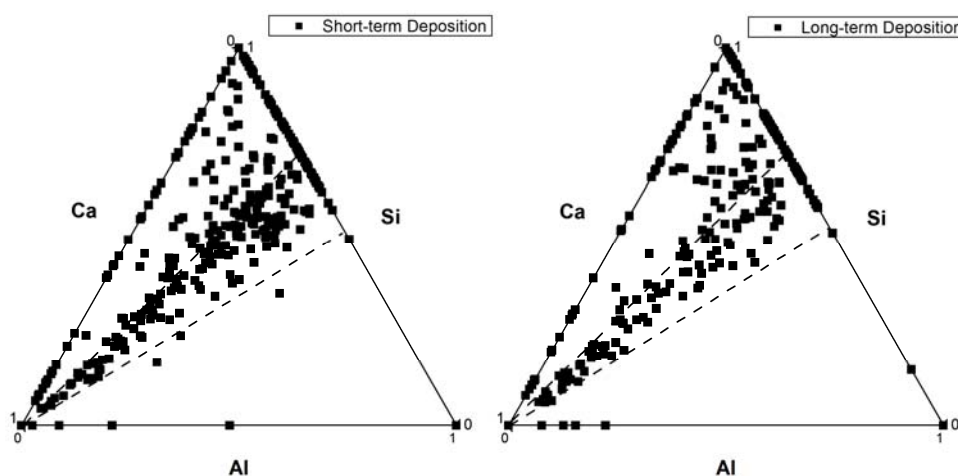
Fig. 1. Relative weight ratios of Al, Si, and Ca for individual dust mineral particles in short-term deposition and long-term deposition samples. Dashed lines from the left corner to the right axis correspond to the mass ratios of Si/Al (2.07 and 1.04) for clay minerals in Chinese loess.

quartz and aluminosilicates (shown by points inside the triangles), or mixed externally (shown by points near the corners and lines). Fugitive dust from the Chinese Loess Plateau comprises quartz and clay minerals such as montmorillonite, illite, chlorite, kaolinite, and muscovite, whose SiO_2/Al_2O_3 molar ratios are 4, 3, 3, 2, and 2, respectively (Wen, 1989; Eden *et al.*, 1994; Kalm *et al.*, 1996). The points where the dashed lines from the left corner intersect the right axis (for Si) show mass ratios for Si/Al of 2.07 and 1.04 (correspondingly, SiO_2/Al_2O_3 molar ratios are 4 and 2), respectively. The locations of most points in Fig. 1 indicate that most deposited particles are quartz and clay minerals from surrounding loess. These particles are mixtures of Ca-containing particles and multiple clays or quartz. The distribution of particles is similar in all samples, suggesting that transport of outdoor fugitive dust into the pit enclosures by natural ventilation and resuspension of deposited dusts caused by visitors are the primary sources of indoor deposition. Fly ashes are characteristic and consistent with aluminosilicate glassy spheres that could have come from Bahe Thermo-electric Plant located 17 km west of the museum. Biogenic particles were almost pollens and spores that probably derived from foliage in the museum courtyards and surrounding agricultural fields. Vehicle emissions from a highway 3 km away may be the dominant source of soot aggregates.

Deposited soot and soil dust in the museum is of particular interest because those species are light-absorbing and can produce visible soiling deposits on the statues. Soil dusts are abrasive and appear brown when deposited on a statue. Soot from vehicle exhausts are characteristically black or gray. Soil dust settles on upward-facing surfaces under the influence of gravity, whereas soot deposits on surfaces of any orientation due to a combination of advective diffusion and thermophoresis (Nazaroff *et al.*, 1993). The wide windows in Pit 1 remain open all year. Consequently, protection of terra-cotta statues from soiling due to the deposition of airborne particles includes alternative control measures, such as mechanical ventilation and effective airborne particle filtration systems, reducing the rate of entry of outdoor particles into the building, managing the museum surroundings to achieve lower outdoor particle concentrations, and adopting proper pavement coverings and display strategies to reduce indoor particle sources from visitor activities.
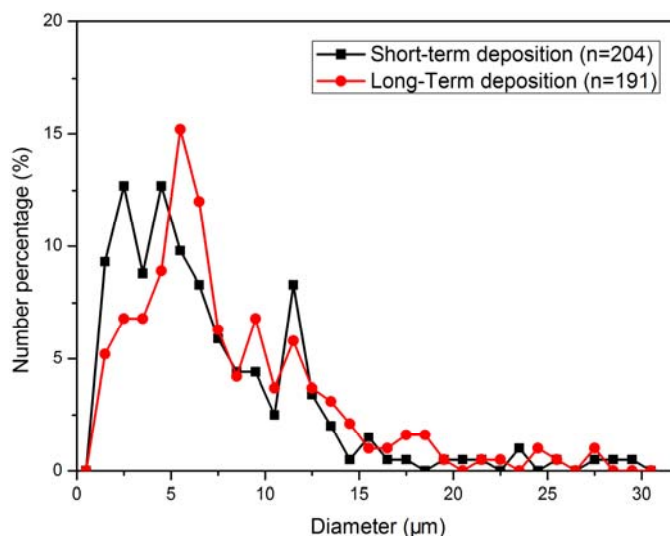
S-Containing Particles

SEM-EDX measurement shows that S-containing particles constituted 51.5% of the short-term deposition particles and 49.5% of the long-term deposition particles with diameters of 1.0–29.0 μm and 1.2–37.7 μm, respectively. The Ca + S particle number fraction is lower in the short-term (12.6%) than in the long-term deposition samples (15.6%). Since the mass ratio of Ca/S in gypsum is 1.25, a dashed line from the right corner to the left axis (Ca) was drawn on ternary plots of Si, S, and Ca in Fig. 2. More S-containing particles in long-term deposition are along this gypsum line than is the case for short-term deposition, indicating that more gypsum particles are in the long-term deposited dust. Impure gypsum particles were in an internally mixed state with clay or quartz. Fig. 3 also illustrates higher number percentages of fine deposition containing S in the short term, indicating that S-containing particles agglomerated with time in settled dust.

Fig. 4 shows floccules of $CaSO_4$ attaching to deposited particles, including silicates (Fig. 4a and 4b), quartz (Fig. 4c), aluminosilicates (Fig. 4d), dolomite (Fig. 4e) and biogenic particles (Fig. 4f). The $CaSO_4$ in Fig. 4 is not a typical component of local soil dust, coal combustion by-products, or construction dust (Wen, 1989; Cao *et al.*, 2005b), and is probably the product of indoor-chemical reactions. Chinese loess has an average calcite content of 12.3% (Wen, 1989) at the QTM location. Sulfur enrichment on particle surfaces has been observed in
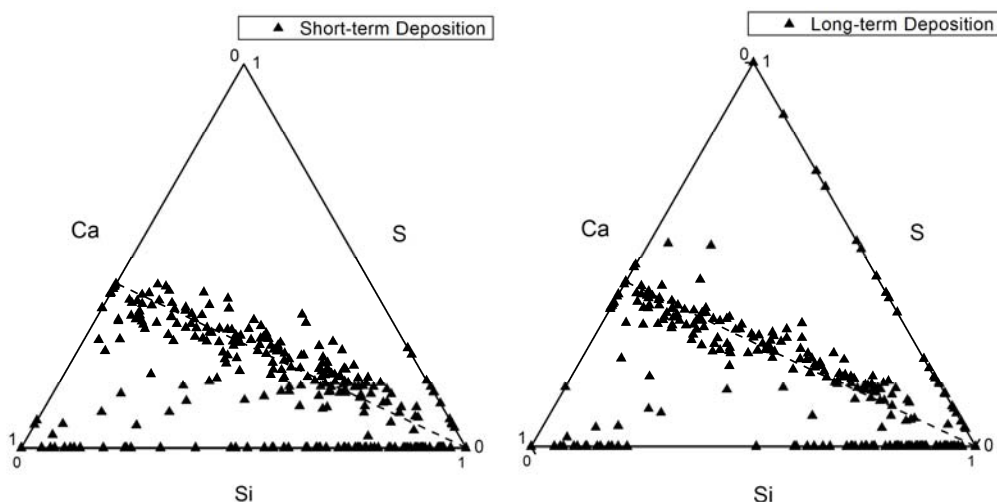
Fig. 2. Relative weight ratios of Si, S, and Ca for individual S-containing particles short-term deposition and long-term deposition samples. Dashed line from the right corner to the left axis corresponds to the mass ratio of Ca/S (1.25) in gypsum.

Fig. 3. Size distribution of S-containing particles in short-term deposition and long-term deposition samples. (The number of detected S-containing particles is in parentheses)
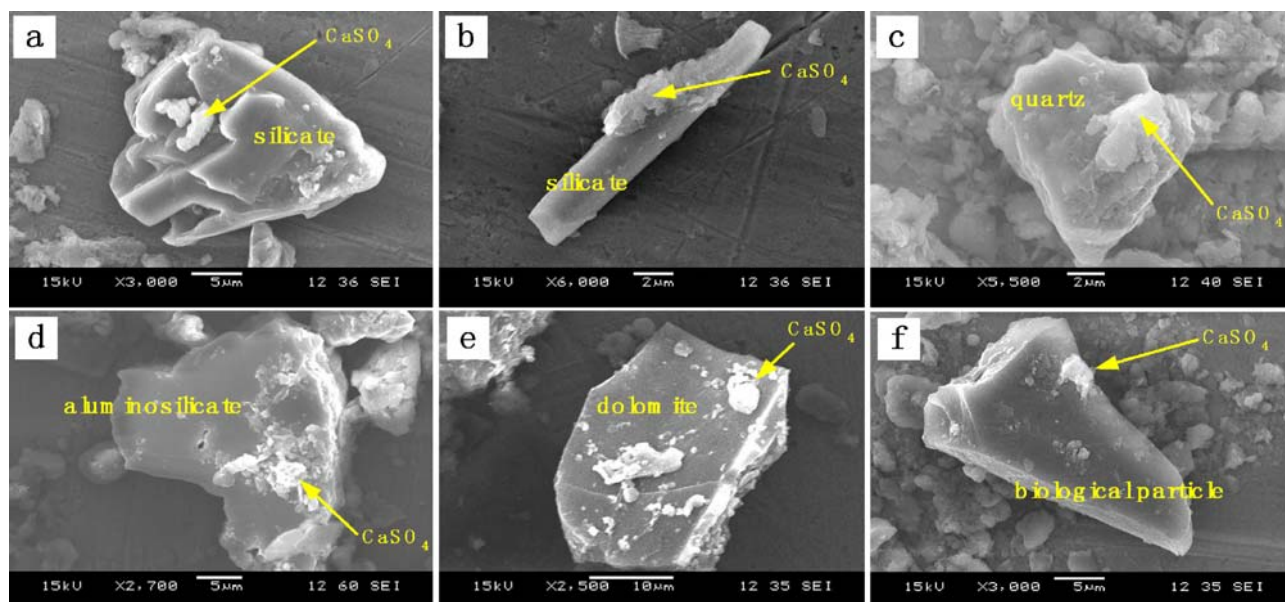
Fig. 4. Floccules of gypsum on multiform particles in QTM. Fig. 4e is from short-term deposition, others are from long-term deposition samples.

aerosol samples collected in other parts of China (Zhang *et al.*, 2000). Jeong and Chun (2006) also found multimineral aggregates of clay and calcite nanofibers in Asian particles. The high surface area of calcite nanofibers may accelerate the reaction with SO_2 or sulfuric acid in the atmosphere during long-term suspension. Indoor and outdoor temperatures, relative humidity, and SO_2 concentration in Pit 1 were measured from April 2006 to April 2007. These have been compared with data obtained in 1989 and 1992 (Zhang, 1998), and August 2004 (Cao *et al.*, 2005a) in Table 2. All the wide windows in Pit 1 remain open all year and indoor conditions are similar to those outdoors except for direct solar illumination. Table 2 shows that the average indoor temperature was 3.5°C higher than the outdoor temperature, and the indoor relative humidity (RH)

reached 80% during summer. The reactions of minerals with atmospheric SO_2 in Pit 1 could be similar to those outdoors (Zhang *et al.*, 2000; Jeong and Chun, 2006).

The principal product of many cultural artifact degradation reactions is gypsum, resulting from the interaction between SO_2 or SO_4^{2-} and $CaCO_3$ in the artifacts (Camuffo *et al.*, 1982). Both simulation chamber and field tests indicate that deposition of fly ash on carbonate stone surfaces leads to the formation of a sulfated black crust (Ausset *et al.*, 1999). Grains of clay (illite and calcite) with small patches of $CaSO_4$ have been observed in Chinese aerosol samples, apparently the result of progressive reactions (Gao and Anderson, 2001). SO_2 could deposit to the surface of particles and form sulfuric acid, activated by subsequent humid conditions with the

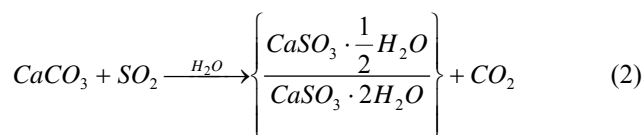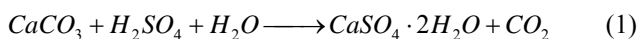**Table 2.** Air quality of indoor and outdoor environment of Pit 1 in QTM.

Monitoring Date	Indoor Temperature (°C)			Outdoor Temperature (°C)			Indoor RH (%)			Outdoor RH (%)			Indoor SO$_2$ (µg/m^3)	Outdoor SO$_2$ (µg/m^3)
	Max.	Min.	Ave.	Max.	Min.	Ave.	Max.	Min.	Ave.	Max.	Min.	Ave.		
04/2006–04/2007 (in this study)	42.0	-5.5	19.6	41.9	-6.8	16.1	87.1	10.2	49.6	100.0	9.0	64.5	27.3 ± 11.89[a]	33.73 ± 17.56[a]
08/2004 (Cao *et al.*, 2005a)	32.4	21.9	26.2	-	-	-	80	56	70.8	-	-	-	-	-
1992 (Zhang, Z.J., 1998)	-	-	13.7	-	-	13.7	-	-	67	-	-	64	33.1 ± 31.2[a,b]	59.25 ± 45.9[a,b]
1989 (Zhang, Z.J., 1998)	-	-	13.8	-	-	13.8	-	-	68	-	-	65	-	-

[a]: mean ± standard deviation; [b]: monitored in 1993; -: not available.

presence of Fe- and/or Mn-containing particles as oxidation catalysts (Brandt and Van Eldik, 1995). Surface corrosion follows reactions Eqs. (1–3) (Rastogi and Sarin, 2006), with the formation of sulfate as an intermediate in the process of sulfation (Gobbi *et al.*, 1998):

$$CaCO_3 + H_2SO_4 + H_2O \longrightarrow CaSO_4 \cdot 2H_2O + CO_2 \qquad (1)$$

$$CaCO_3 + SO_2 \xrightarrow{H_2O} \left\{ \begin{array}{l} CaSO_3 \cdot \frac{1}{2}H_2O \\ \overline{CaSO_3 \cdot 2H_2O} \end{array} \right\} + CO_2 \qquad (2)$$

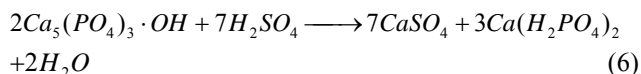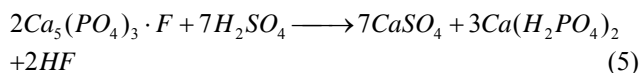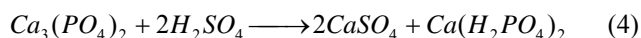$$CaSO_3 \cdot 2H_2O + O_2 \longrightarrow CaSO_4 \cdot 2H_2O \qquad (3)$$

The terra-cotta statues are composed of porous pottery with long-term weatherability. However, dissolved substances can penetrate the porous surface and move inside driven by capillary and adsorption forces (Cardell *et al.*, 2003). Inside the terra-cotta statues, formation, accumulation, hydration, crystallization, dissolution, penetration, and recrystallization of gypsum may cause chemical and structural changes. The solubility of gypsum in water is higher than that of calcite (2.4 versus 0.014 g/L) (Van Grieken *et al.*, 1998; Brimblecombe, 2003), which is an important component of terra-cotta statues (Zhang, 1998). According to records from 1989 and 1992, the daily averaged temperature fluctuated from –4.2°C to 32°C in Pit 1, with daily averaged RH from 35% to 92% (Zhang, 1998). Daily averaged temperature and RH fluctuations during 2006–2007 were –5.5°C to 42°C, and 10.2% to 87.1%, respectively (Table 2). At higher RH, fine grains of gypsum can dissolve and penetrate into the inner pores of the statues. After evaporation of water, these salts recrystallize and cause stress within the statues. Investigations of calcareous stone weathering also show that physical stress resulting from salt crystallization in pores is an important mechanism causing breakage of stone (Cardell *et al.*, 2003).

CaSO$_4$ on the Pigment Flakes

Apatite appears to be the mineral pigment material used on the faces of terra-cotta warriors (Zhang, 1998). Fig. 5 shows remnants of pigment flakes on the face of a partially restored warrior. SEM images show small pits and cracks on the inner and outer surfaces of pigment samples, with mineral, fly ash, and biogenic particles scattered irregularly around the pits. Near the interconnected pits and cracks, gypsum crystals (highlighted by rectangles) are growing from the apatite particles of the outer surface of pigment flakes (Fig. 6). EDX analyses indicated that the crystals contained O, P, S, and Ca, with a minor amount of crustal elements such as Si and Al. Apatite can react with sulfuric acid as shown in Eqs. (4–6):

$$Ca_3(PO_4)_2 + 2H_2SO_4 \longrightarrow 2CaSO_4 + Ca(H_2PO_4)_2 \qquad (4)$$

$$2Ca_5(PO_4)_3 \cdot F + 7H_2SO_4 \longrightarrow 7CaSO_4 + 3Ca(H_2PO_4)_2 + 2HF \qquad (5)$$

$$2Ca_5(PO_4)_3 \cdot OH + 7H_2SO_4 \longrightarrow 7CaSO_4 + 3Ca(H_2PO_4)_2 + 2H_2O \qquad (6)$$

The development of gypsum crystals has been observed in close proximity with fly ash, anchoring the fly ash to the limestone surfaces (Ausset *et al.*, 1999). Weathering tests also show chemical deterioration by gypsum in glassy crusts. When the crusts were removed, a highly cracked surface was observed in the potassic glasses (Carmona *et al.*, 2005). The crystallization, dissolution, penetration and recrystallization of gypsum with the fluctuation of RH and temperature may produce stress, thereby causing pits, cracks and, ultimately, flaking of pigments.

CONCLUSION

SEM-EDX morphological and elemental analyses of indoor dust deposition and pigment flakes collected in Pit 1 of the QTM characterized the physical and chemical components with deposited particles as well as damaged surfaces on the terra-cotta warriors. Gypsum particles were more frequently observed in long-term deposited dust, which probably resulted from deposition of SO$_2$ in the museum onto dust surfaces with subsequent reactions.

Fig. 5. Pigment flakes on the face of a partially restored terra-cotta warrior.
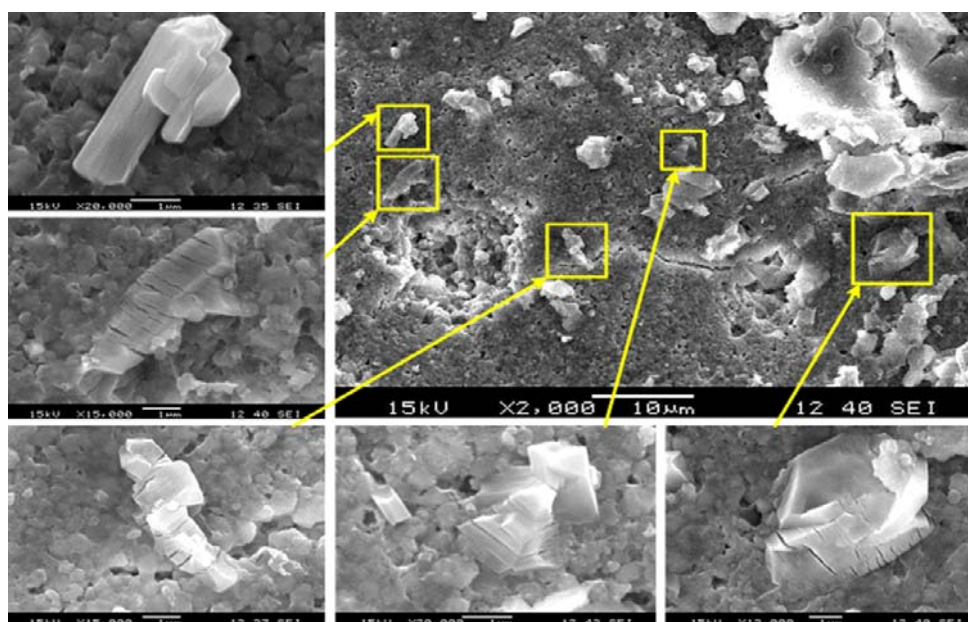
Fig. 6. Neo-formed rystals of gypsum (highlighted by rectangles) near pits and cracks on the surface of a pigment flake. The smaller photographs are magnified SEM images of the crystals situated in rectangles, indicated by the arrows.

Microscopic examination showed gypsum floccules on deposited particles and on the front and back of pigment flakes. Gypsum crystals were found near interconnected pits and cracks on both sides of the pigment flaked off the faces of warrior statues. Under variable temperature and RH conditions inside the museum, the gypsum particles, which appear to be the product of chemical reactions between atmospheric SO_2 and apatite or deposition particles on pigment layers, play an important role in the formation of pits and cracks on the surface of pigment flakes.

REFERENCES

Ausset, P., Del Monte, M. and Lefèvre, R.A. (1999). Embryonic Sulphated Black Crusts on Carbonate Rocks in Atmospheric Simulation Chamber and in the Field: Role of Carbonaceous Fly-Ash. *Atmos. Environ.* 33: 1525-1534.

Brandt, C. and Van Eldik, R. (1995). Transition Metal-Catalysed Oxidation of Sulfur (IV) Oxides: Atmospheric-Relevant Processes and Mechanisms. *Chem. Rev.* 95: 119-190.

Brimblecombe, P. (1990). The Composition of Museum Atmospheres. *Atmos. Environ.* 24: 1-8.

Brimblecombe, P. (2003). *The Effects of Air Pollution on the Built Environment*, Imperial College Press, London.

Camuffo, D., Del Monte, M., Sabbioni, C. and Vittori, O.

(1982). Wetting Deterioration and Visual Features of Stone Surfaces in an Urban area. *Atmos. Environ.* 16: 2253-2259.

Cao, J.J., Rong, B., Lee, S.C., Chow, J.C., Ho, K.F., Liu, S.X. and Zhu, C.S. (2005a). Composition of Indoor Aerosols at Emperor Qin's Terra-Cotta Museum, Xi'an, China, during Summer, 2004. *China Particuology.* 3: 170-175.

Cao, J.J., Lee, S.C., Zhang, X.Y., Chow, J.C., An, Z.S., Ho, K.F., Watson, J.G., Fung, K., Wang, Y.Q. and Shen, Z.X. (2005b). Characterization of Airborne Carbonate over a Site on Asian Dust Source Regions during 2002 Spring and Its Climatic and Environmental Significance. *J. Geophys. Res.* 110: D03203.

Cardell, C., Delalieux, F., Roumpopoulos, K., Moropoulou, A., Auger, F. and Van Grieken, R. (2003). Salt-Induced Decay in Calcareous Stone Monuments and Building in a Marine Environment in SW France. *Constr. Build. Mater.* 17: 165-179.

Carmona, N., Villegas, M.A. and Fernández Navarro, J.M. (2005). Corrosion Behaviour of R_2O–CaO–SiO_2 Glasses Submitted to Accelerated Weathering. *J. Eur. Ceram. Soc.* 25: 903-910.

De Bock, L.A., Van Grieken, R.E., Camuffo, D. and Grime, G.W. (1995). Microanalysis of Museum Aerosols to Elucidate the Soiling of Paintings: Case of the Correr Museum, Venice, Italy. *Environ. Sci. Technol.* 30: 3341-3350.

Eden, D.N., Wen, Q., Hunt, J.L. and Whitton, J.S. (1994). Mineralogical and Geochemical Trends across the Loess Plateau, North China. *Catena.* 21: 73-90.

Gao, Y. and Anderson, J.R. (2001). Characteristics of Chinese Aerosols Determined by Individual-Particle Analysis. *J. Geophys. Res.* 106: 18037-18045.

Gobbi, G., Zappia, G. and Sabbioni, C. (1998). Sulphite Quantification on Damaged Stones and Mortars. *Atmos. Environ.* 32: 783-789.

Jeong, GY and Chun, Y. (2006). Nanofiber Calcite in Asian Dust and Its Atmospheric roles. *Geophys. Res. Lett.* 33: L24802.

Kalm, V.E., Rutter, N.W. and Rokosh, C.D. (1996). Clay Minerals and Their Paleoenvironmental Interpretation in the Baoji Loess Section, Southern Loess Plateau, China. *Catena.* 27: 49-61.

Katsanos, N.A., De Santis, F., Cordoba, A., Roubani-Kalantzopoulou, F. and Pasella, D. (1999). Corrosive Effects from the Deposition of Gaseous Pollutants on Surfaces of Cultural and Artistic Value Inside Museums. *J. Hazard. Mater.* 64: 21-36.

Nazaroff, W.W. and Cass, G.R. (1991). Protecting Museum Collections from Soiling due to the Deposition of Airborne Particles. *Atmos. Environ.* 25: 841-852.

Nazaroff, W.W., Ligocki, M.P., Salmon, L.G., Cass, G.R., Fall, T., Jones, M.C., Liu, H.I.H. and Ma, T. (1993). *Airborne Particles in Museums*, Research in Conservation 6. Getty Conservation Institute, Los Angeles, p. 17.

Okada, K. and Kai, K. (2004). Atmospheric Mineral Particles Collected at Qira in the Taklamakan Desert, China. *Atmos. Environ.* 38: 6927-6935.

Rastogi, N. and Sarin, M.M. (2006). Chemistry of Aerosols over a Semi-Arid Region: Evidence for Acid Neutralization by Mineral Dust. *Geophys. Res. Lett.* 33: L23815.

Van Grieken, R., Delalieux, F. and Gysels, K. (1998). Cultural Heritage and the Environment. *Pure Appl. Chem.* 70: 2327-2331.

Wen, Q.Z. (1989). *Chinese Loess Geochemistry.* Science Press, Beijing. (in Chinese)

Yoon, Y.H. and Brimblecombe, P. (2001). The Distribution of Soiling by Coarse Particulate Matter in the Museum Environment. *Indoor Air.* 11: 232-240.

Zhang, D.Z., Shi, G.Y., Iwasaka, Y. and Hu, M. (2000). Mixture of Sulfate and Nitrate in Coastal Atmospheric Aerosols: Individual Particle Studies in Qingdao (36°04'N, 120°21'E), China. *Atmos. Environ.* 34: 2669-2679.

Zhang, D.Z., Zang, J.Y., Shi, G.Y., Iwasaka, Y., Matsuki, A. and Trochkine, D. (2003). Mixture State of Individual Asian Dust Particles at a Coastal Site of Qingdao, China. *Atmos. Environ.* 37: 3895-3901.

Zhang, Z.J. (1998). *Study on Conservation of Qin Terra-Cotta Army.* Shaanxi People Education Press, Xi'an. (in Chinese)